

Numerical Study of Forced Convection Heat Transfer Across an Elliptic Cylinder in Laminar and Unsteady Nanofluid Flow

Hamdy M. Kotb, Fathy M. Mahfouz, and Mohamed A. Abdel-Majeed*

Department of Mechanical Power Eng., Shebin Faculty of Eng., Menoufia University, Egypt.

**(Corresponding author: mohaelano@gmail.com)*

ABSTRACT

This paper investigates theoretically forced convection from an inclined elliptic cylinder placed in a nanofluid cross laminar flow with constant surface temperature. The nanofluid is created by suspending copper particles in water. The referred problem is studied through solving the conservation equations of mass, momentum, and energy using Fourier spectral method. There are some important parameters affect the heat transfer characteristics which can be presented as follows: Inclination angle which varies from 0 to 90 degrees, and copper nanoparticles volume fraction starts from 0 up to 0.05. these parameters are investigated under the conditions: Reynolds number is 50, elliptic axis ratio is fixed at 0.5, and constant surface temperature. The results are found to be in a good agreement with the previous studies in the same category, for different axes ratios and Prandtl number of 0.7. The conclusions of the present investigation show that when nanoparticles volume fraction increases, an obvious enhancement in heat transfer is produced. On the other hand, when changing the angle of inclination from 0 up to 90 the flow exhibits lower heat transfer rates, and all these results are indicated through calculating average Nusselt number.

Keywords: *Nanofluid, Forced Convection, Unsteady, Elliptical Cylinder, Over Flow*

1. Introduction

Numerous industrial applications include forced convection heat transfer from cylinders with circular and non-circular cross sections, such as elliptic, such as in boilers, heat exchangers, thermal storage systems, solar heating systems, nuclear reactor cooling, electronics and so forth. Due to these extensive applications in a variety of industrial contexts, significant research efforts have been conducted to study the forced convection heat transfer from cylinders with different cross sections. These efforts have used both theoretical and experimental methods.

Much research work has been expended on ways to enhance the heat transfer characteristics of the conventional fluids employed in these applications, such as water. To that end, a new class of fluid known as 'nanofluids' is now widely employed in a variety of applications, such as heat exchangers, condensers, and evaporators. Such fluids are produced by dispersing nanoparticles of metals or their oxides in a base fluid such as water, and the resulting fluid has superior heat conduction capabilities than a conventional fluid [1]. Choi and Eastman [2] used suspended metallic nanoparticles in the base fluid in a heat exchanger and claimed that the heat transfer characteristics have been improved and so Humnic and Humnic[3] reviewed

many articles prove that heat transfer is enhanced when nanofluids are used, basically in heat exchangers' applications. Saidur et al. [4] made a review on applications and challenges of nanofluids, whereas Rashidi et al. [5] have investigated applications of nanofluids in condensing and evaporating systems.

There is a significant amount of literature available on forced convection from an elliptic cylinder placed in basic fluids (such as air or water), for example, see Refs [6, 7, 8 and 9].

In contrast, for nanofluids, recently, an inclined elliptic tube with a constant aspect ratio of 0.5 submerged in a flowing water based Al₂O₃ nanofluid was studied by Sasmal [10], particularly, gives extensive numerical data for the following conditions: The Reynolds number ranges from 0.01 to 40, the cylinder inclination angle ranges from 0 to 90, and the nanoparticle volume fraction ranges from 0% to 6%. He claimed that The Nusselt number and drag force both rise with nanoparticle volume fraction, and the average Nusselt number increases with increasing inclination angle. The numerical study of steady forced convection of water-based nanofluids around an elliptic cylinder by Khan et al [11]. Copper (Cu) and aluminum oxide (Al₂O₃) nanoparticles were mixed into the water to improve heat transfer. The

governing equations are numerically solved using the Runge-Kuta-Fehlberg technique of seventh order and enhanced by the shooting method. The study deduced that the local Nusselt number is found to be increased with increasing solid volume fraction of nanoparticles and with axis ratio increasing. Apart from elliptic cylinders, numerical study of forced convection from a steady rotating circular cylinder in a nanofluid flow has been carried out by Mahfouz et al. [12]. The Reynolds number is considered up to 200, and the volume fraction of nanoparticles is up to 5%. According to the findings, increasing the volume fraction of nanoparticles boosts the heat transfer rate for both fixed and rotating cylinder.

It has been observed that the overall rate of heat transfer is significantly influenced by the cross-sectional area of a cylinder, its orientation, and the type of fluid. The main objective of this paper is to conduct a thorough investigation of how the angle of inclination and nanoparticle volume fraction affects the heat transfer through an elliptic cylinder as there is a lack in the previous studies for this case.

2. Problem Formulation

2.1 Governing equations and boundary conditions

In this work, consider unsteady laminar flow of a nanofluid over an elliptical tube with a length assumed to be infinite. The elliptical cross-section is described by b and a which refer to the minor and major axes as illustrated in geometry of the flow, Figure (1) and the figure shows also the cartesian and elliptic coordinates. Cylinder surface has a constant temperature of T_s and inclined to the flow direction with an angle λ . The far stream velocity of the nanofluid is U_∞ and have a uniform temperature of T_∞ .

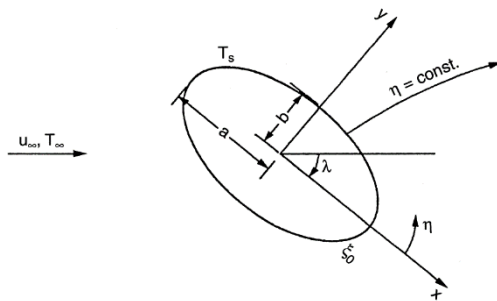


Figure 1- Schematic representation of flow over an elliptic cylinder and coordinates system

Assuming 2D unsteady convective nanofluid flow, nanoparticles are assumed to be uniform shape and size, and neglecting buoyancy force. The governing equations, based on the previous assumptions, of motion and energy in Cartesian coordinates is given as

follows:

$$\frac{\partial \zeta}{\partial t} + u \frac{\partial \zeta}{\partial x} + v \frac{\partial \zeta}{\partial y} = \frac{2}{\text{Re}} \nabla^2 \zeta \quad (1)$$

$$\zeta - \nabla^2 \psi = 0 \quad (2)$$

$$\frac{\partial \phi}{\partial t} + u \frac{\partial \phi}{\partial x} + v \frac{\partial \phi}{\partial y} = \frac{2}{\text{RePr}} \nabla^2 \phi \quad (3)$$

The velocities are defined as

$$u = \frac{\partial \psi}{\partial y}, \quad v = -\frac{\partial \psi}{\partial x}$$

Where u and v are the components of the velocity in the directions of x and y axes, Re , Pe and Pr are the Reynolds number, Peclet number and Prandtl number, respectively, (based on the cylinder diameter and the velocity of free stream). ϕ represents the dimensionless temperature, ψ is the stream function, and ζ represents the vorticity. All dimensionless parameters maybe expressed related to the dimensional parameters with primes as follows:

$$x = \frac{x'}{c}, \quad y = \frac{y'}{c}, \quad u = \frac{u'}{U_\infty}, \quad v = \frac{v'}{U_\infty}$$

$$t = \frac{U_\infty t'}{c}, \quad \psi = \frac{\psi'}{cU_\infty}, \quad \zeta = -\frac{\zeta' c}{U_\infty}, \quad \phi = \frac{T - T_\infty}{T_s - T_\infty}$$

Reynolds and Peclet numbers are defined

$$\text{Re} = \frac{2U_\infty c}{\nu} \quad \text{and} \quad \text{Pe} = \text{Re} \cdot \text{Pr}$$

Where ν stands for the kinematic viscosity, and c is the focal distance

Applying the transformation from the Cartesian to the elliptical coordinates (ξ, η) is needed to achieve an acceptable model and that could be done through

$$x = c \cosh \xi \cos \eta \quad \text{and} \quad y = c \sinh \xi \sin \eta$$

The governing equations (1), (2), and (3) are converted through the transformation

$$H \frac{\partial \zeta}{\partial t} = \frac{\partial \psi}{\partial \xi} \frac{\partial \zeta}{\partial \eta} - \frac{\partial \psi}{\partial \eta} \frac{\partial \zeta}{\partial \xi} + \frac{2}{\text{Re}} \nabla^2 \zeta \quad (4)$$

$$H \zeta - \nabla^2 \psi = 0 \quad (5)$$

$$H \frac{\partial \phi}{\partial t} = \frac{\partial \psi}{\partial \xi} \frac{\partial \phi}{\partial \eta} - \frac{\partial \psi}{\partial \eta} \frac{\partial \phi}{\partial \xi} + \frac{2}{\text{Pe}} \nabla^2 \phi \quad (6)$$

Where

$$\nabla^2 = \frac{\partial^2}{\partial \xi^2} + \frac{\partial^2}{\partial \eta^2}, \quad H = \frac{1}{2}(\cosh 2\xi - \cos 2\eta)$$

From the no slip and isothermal conditions at cylinder wall ($\xi = \xi_0$) and the far stream conditions ($\xi \rightarrow \xi_\infty$) the boundary conditions can be expressed in the new coordinates as

$$\psi = \frac{\partial \psi}{\partial \xi} = \frac{\partial \psi}{\partial \eta} = 0, \quad \phi = 1 \quad \text{when } \xi = \xi_0 \quad (7a)$$

$$\frac{\partial \psi}{\partial \xi} \rightarrow -\frac{1}{2} e^\xi \sin(\lambda - \eta), \quad \zeta \rightarrow 0 \quad \text{as } \xi \rightarrow \infty \quad (7b)$$

$$\frac{\partial \psi}{\partial \eta} \rightarrow \frac{1}{2} e^\xi \cos(\lambda - \eta), \quad \phi = 0 \quad \text{as } \xi \rightarrow \infty \quad (7c)$$

Where the constant ξ_0 is defined by $\xi_0 = \tanh^{-1}(\text{AR})$, and AR is the Axis ratio $\text{AR} = b/a$.

The Navier–Stokes and energy equations (4), (5) and (6) are ready to be solved now using the spectral method but first we need to approximate the vorticity, stream function and temperature using the expansion series of Fourier as follows:

$$\psi = \frac{1}{2} F_0(\xi, t) + \sum_{n=1}^N f_n(\xi, t) \sin n\eta + F_n(\xi, t) \cos n\eta \quad (8a)$$

$$\zeta = \frac{1}{2} G_0(\xi, t) + \sum_{n=1}^N g_n(\xi, t) \sin n\eta + G_n(\xi, t) \cos n\eta \quad (8b)$$

$$\phi = \frac{1}{2} H_0(\xi, t) + \sum_{n=1}^N h_n(\xi, t) \sin n\eta + H_n(\xi, t) \cos n\eta \quad (8c)$$

Applying the above series to the governing equations (4), (5), and (6), multiplying each side times $\{1, \sin n\eta, \cos n\eta : n=1, 2, \dots\}$ and the integrating from 0 to 2π with respect to η we can find that:

$$\frac{\partial^2 F_0}{\partial \xi^2} = \frac{1}{2} [(\cosh 2\xi) G_0 - G_2] \quad (9a)$$

$$\frac{\partial^2 F_n}{\partial \xi^2} - n^2 F_n = \frac{1}{2} (\cosh 2\xi) G_n - \frac{1}{4} [G_0 \delta_{n2} + G_{|n-2|} + G_{(n+2)}] \quad (9b)$$

$$\frac{\partial^2 f_n}{\partial \xi^2} - n^2 f_n = \frac{1}{2} (\cosh 2\xi) g_n - \frac{1}{4} [\text{sgn}(n-2) g_{|n-2|} + g_{(n+2)}] \quad (9c)$$

$$\frac{1}{2} \left[(\cosh 2\xi) \frac{\partial G_0}{\partial t} - \frac{\partial G_2}{\partial t} \right] = \left(\frac{2}{\text{Re}} \right) \frac{\partial^2 G_0}{\partial \xi^2} + S_{n0}(\xi, t) \quad (10a)$$

$$\left[(\cosh 2\xi) \frac{\partial G_n}{\partial t} - \frac{1}{2} \left[\frac{\partial G_0}{\partial t} \delta_{n2} + \frac{\partial G_{|n-2|}}{\partial t} + \frac{\partial G_{n+2}}{\partial t} \right] \right] = \frac{4}{\text{Re}} \left[\frac{\partial^2 G_n}{\partial \xi^2} - n^2 G_n \right] + n g_n \frac{\partial F_0}{\partial \xi} - n f_n \frac{\partial G_0}{\partial \xi} + S_{n1}(\xi, t) \quad (10b)$$

$$\left[(\cosh 2\xi) \frac{\partial g_n}{\partial t} - \frac{1}{2} \text{sgn}(n-2) \frac{\partial g_{|n-2|}}{\partial t} - \frac{1}{2} \frac{\partial g_{n+2}}{\partial t} \right] = \frac{4}{\text{Re}} \left[\frac{\partial^2 g_n}{\partial \xi^2} - n^2 g_n \right] + n F_n \frac{\partial G_0}{\partial \xi} - n G_n \frac{\partial F_0}{\partial \xi} + S_{n2}(\xi, t) \quad (10c)$$

$$\frac{1}{2} \left[(\cosh 2\xi) \frac{\partial H_0}{\partial t} - \frac{\partial H_2}{\partial t} \right] = \left(\frac{2}{\text{Re}} \right) \frac{\partial^2 H_0}{\partial \xi^2} + Z_{n0}(\xi, t) \quad (11a)$$

$$\begin{aligned} & \left[(\cosh 2\xi) \frac{\partial H_n}{\partial t} - \frac{1}{2} \left[\frac{\partial H_0}{\partial t} \delta_{n2} + \frac{\partial H_{|n-2|}}{\partial t} + \frac{\partial H_{n+2}}{\partial t} \right] \right] \\ & = \frac{4}{Re} \left[\frac{\partial H_n}{\partial \xi^2} - n^2 H_n \right] + n h_n \frac{\partial F_0}{\partial \xi} \\ & - n f_n \frac{\partial H_0}{\partial \xi} + Z_{n1}(\xi, t) \quad (11b) \end{aligned}$$

$$\begin{aligned} & \left[(\cosh 2\xi) \frac{\partial h_n}{\partial t} - \frac{1}{2} \operatorname{sgn}(n-2) \frac{\partial h_{|n-2|}}{\partial t} - \frac{1}{2} \frac{\partial h_{n+2}}{\partial t} \right] \\ & = \frac{4}{Re} \left[\frac{\partial^2 h_n}{\partial \xi^2} - n^2 h_n \right] + n F_n \frac{\partial H_0}{\partial \xi} \\ & - n H_n \frac{\partial F_0}{\partial \xi} + Z_{n2}(\xi, t) \quad (11c) \end{aligned}$$

Where δ_{mn} is the Kronecker delta which can be defined as

$$\delta_{mn} = 1 \text{ if } m = n, \delta_{mn} = 0, \text{ if } m \neq n$$

And the terms S_{nT} and Z_{nT} are identifiable functions of t and ξ where T varies (1,2, and 3). Equations (9a) to (9c), (10a) to (10c) and (11a) to (11c) are three sets of P.D.E.s and each set of $(2N + 1)$ need to be solved, and N is the last term order in the series of Fourier.

2.2 Boundary Conditions

We can describe the above boundary conditions in equations (7a), (7b) and (7c) using Fourier series (8a), (8b) and (8c) resulting:

$$\begin{aligned} F_0 = \frac{\partial F_0}{\partial \xi} = f_n = \frac{\partial f_n}{\partial \xi} = F_n = \frac{\partial F_n}{\partial \xi} = h_n = H_n = 0 \\ H_0=2 \text{ when } \xi = \xi_0 \quad (12a) \end{aligned}$$

$$H_0, H_n, h_n, G_0, g_n, G_n \rightarrow 0 \quad \text{as } \xi \rightarrow \infty \quad (12b)$$

$$F_0 \rightarrow 0, f_n \rightarrow \frac{1}{2} e^{\xi} \cos(\lambda) \delta_{n1} \quad \text{as } \xi \rightarrow \infty \quad (12c)$$

$$F_n \rightarrow -\frac{1}{2} e^{\xi} \sin(\lambda) \delta_{n1} \quad \text{as } \xi \rightarrow \infty \quad (12d)$$

From the conditions (12a) to (12d) and equations (9a), (9b) and (9c) we may have the integral conditions as shown

$$\int_{\xi_0}^{\infty} \{(\cosh 2\xi) G_0 - G_2\} d\xi = 0 \quad (13a)$$

$$\begin{aligned} & \int_{\xi_0}^{\infty} \left(\frac{1}{2} (\cosh 2\xi) G_n \right. \\ & \left. - \frac{1}{4} (G_0 \delta_{n2} + G_{|n-2|} + G_{n+2}) \right) e^{-n\xi} d\xi \\ & = -\sin \alpha \delta_{n1} \quad (13b) \end{aligned}$$

$$\begin{aligned} & \int_{\xi_0}^{\infty} \left(\frac{1}{2} (\cosh 2\xi) g_n \right. \\ & \left. - \frac{1}{4} (\operatorname{sgn}(n-2) g_{|n-2|} + g_{n+2}) \right) e^{-n\xi} d\xi \\ & = \cos \alpha \delta_{n1} \quad (13c) \end{aligned}$$

The above equations 13a, 13b and 13c are used when calculating the boundary conditions at cylinder surface of G_0, G_n and g_n at every step of time.

2.3 Solution Procedure

The governing Equations from (9a) to (11c) are numerically solved using the iterative procedure method of Crank-Nicolson by employing a finite difference type of spatial discretization to each P.D.E. Reynolds number has a value of 50. Furthermore, volume fraction of nanoparticles varies within the range of (0 to .05). The numerical scheme to be used here to generate the solution of the main parameters is the same of that used by Dennis[13]. The different tube geometry, the co-ordinates system and the fluid properties are the main differences here.

The principle of solving is to set all the differential equations in the form:

$$\begin{aligned} \frac{\partial X_n}{\partial T} = a_n \frac{\partial^2 X_n}{\partial \xi^2} + b_n \frac{\partial X_n}{\partial \xi} + c_n X + d_n \\ = q_n(\xi, T) \quad (14) \end{aligned}$$

where a_n, b_n, c_n and d_n are easily identifiable functions of ξ and T . The method of solution used is the Crank-Nicolson implicit method, which can be written as

$$\begin{aligned} X(\xi, T) - \frac{1}{2} h q_n(\xi, T) = X(\xi, T - h) \\ + \frac{1}{2} h q_n(\xi, T - h) \quad (15) \end{aligned}$$

where h is the integration step in the T direction. Central differences are used to approximate the space derivatives

$$\begin{aligned}
 h^2 q_n(\xi, T) = & \\
 & \left(a_n(\xi, T) + \frac{1}{2} h b_n(\xi, T) \right) X(\xi + dx, T) \\
 & + \left(a_n(\xi, T) - \frac{1}{2} h b_n(\xi, T) \right) X(\xi - dx, T) \\
 & + (h^2 c_n(\xi, T) - 2a_n(\xi, T)) X(\xi, T) \\
 & + h^2 d_n(\xi, T) \quad (16)
 \end{aligned}$$

And substituting in the main differential equations using the above expression could lead us to have a tri-diagonal matrix in the form

$$\begin{aligned}
 A_n(\xi, T) X(\xi - dx, T) + B_n X(\xi, T) \\
 + C_n(\xi, T) X(\xi + dx, T) = D_n(\xi, T) \quad (17)
 \end{aligned}$$

The right-hand side is considered known through applying the deduced condition

The above cycle from $n = 1$ to N is repeated until, ultimately, convergence is achieved. This is decided by the test

$$|X^{(m+1)}(\xi, T) - X^{(m)}(\xi, T)| > 10^{-5} \quad (18)$$

For all $n = 1, 2, 3, \dots, N$ and for all grid values of ξ throughout the field, i.e. $\xi = 0, dx, 2dx, \dots, L$. Here, the superscripts (m) and $(m + 1)$ refer to two successive iterates in the cyclic procedure.

The above procedure is done to get all the functions in the whole domain to secure obtaining the properties at every single point in the time and space domain. And the procedure us introduced in the flow chart Figure (2).

2.3 Nanofluids thermo-physical properties

The physical properties of pure copper and water at average atmospheric temperature are obtained from [14] and presented in Table (1).

Table 1- Thermophysical properties of pure water and copper at room temperature.

Material	ρ (kg/m ³)	μ (kg/ms)	k (w/m.K)	C_p (J/kg.K)
Water	997.1	0.001	0.6	4179
Copper	8954	-	400	383

We assume Brinkman [15] model for computing effective viscosity of the nano-fluid. The expression for effective viscosity is given by,

$$\mu_{nf} = \frac{\mu_f}{(1-\phi_p)^{2.5}} \quad (19)$$

and ϕ_p here refers to the volume fraction of nanoparticles related to the total liquid volume

$$\phi_p = \frac{\text{Volume of solid (nano) particles}}{\text{Total volume of nanofluid}} \quad (20)$$

Above correlation was validated by Xuan and Li[16] for copper nanoparticles with water as a base fluid. Their experiment gave good results that match with Brinkman model. Effective density of the nano-fluid at reference temperature is given by:

$$\rho_{nf} = \phi_p \rho_p + (1 - \phi_p) \rho_f \quad (21)$$

Where ρ_p is the density of the solid nanoparticles at reference temperature, and ρ_f is the density of the base fluid at reference temperature. The effective heat capacitance of the nano-fluid at the reference temperature is calculated by the equation given by Xuan and Li[16] as given bellow.

$$(\rho C_p)_{nf} = \phi_p (\rho C_p)_p + (1 - \phi_p) \cdot (\rho C_p)_f \quad (22)$$

The effective thermal conductivity is determined using the model of Maxwell-Garnett's[14] especially for two phase solution and the shape of nanoparticles is spherical and is expressed below

$$k_{nf} = k_f \left[\frac{(k_p + 2k_f) - 2\phi_p(k_f - k_p)}{(k_p + 2k_f) + \phi_p(k_f - k_p)} \right] \quad (23)$$

It is important to mention here that Maxwell–Garnett’s model and Brinkman model is the basic model for micro-suspension and is restricted to spherical particles only. Accordingly, the present theoretical consideration has been kept simple with the use of basic models available in literature and the effective thermal conductivity and effective viscosity of the nano-fluid is approximated by Maxwell–Garnett model and Brinkman model respectively, within the domain of the single-phase formulation approach . Notice that a similar approach was previously used by earlier researchers [21] and [22] to model the effective thermo-physical properties of the nanoparticle suspension. Such an approach also finds experimental

confirmation in the data reported by Xuan and Li [9] for Cu–water and oil–water nano-fluids. The thermo-physical properties of the nano-fluids are assumed to be constant.

We can express the thermal diffusion by expressing diffusivity.

$$\alpha_{nf} = \frac{k_{nf}}{(\rho c_p)_{nf}} \quad (24)$$

2.4 Important analysis parameters

We need to introduce some important parameters to expand our analysis of the present study in details. For instance, Nusselt number: it is our heat transfer indicator, and we can express it as a local value (Nu) deduced from the convective heat transfer coefficient

$$h = -\frac{k_{nf}}{c} \left(\frac{\partial \phi}{\partial \xi} \right)_{\xi_0} \quad (25 \text{ a})$$

$$Nu = \frac{2ch}{k_f} = -\frac{2 \cosh \xi_0}{H \frac{1}{\xi_0}} \left(\frac{\partial \phi}{\partial \xi} \right)_{\xi_0} \cdot \frac{k_{nf}}{k_f} \quad (25 \text{ b})$$

And the Nusselt number as an average value (\bar{Nu}) is obtained from

$$\bar{Nu} = \frac{1}{L} \int_0^L Nu. ds = -\frac{2\pi}{(L/a)} \left(\frac{\partial \phi}{\partial \xi} \right)_{\xi_0} \cdot \frac{k_{nf}}{k_f} \quad (26)$$

3. Results and discussion

In the beginning and before presenting the study results, it is unavoidable to check the accuracy of the method of solution. By overviewing the previous work in the same category, some studies’ results are found to be trustable to compare with. These studies are investigated under the following conditions, forced convection, cross flow, stationary cylinder with circular cross section, Pr=0.6, Re=5, 20 and 40 and constant surface temperature The axis ratio AR in the present study needs to be limited to a value to turn the elliptical section to be so close to the circular cylinder to take almost the same conditions of comparative studies and that could be achieved by putting AR close to the unity (AR=0.97). The compared results are illustrated in table (2) where the face of comparison is the average Nusselt number. By comparing the results an average variation from each comparative could be calculated. Differences from each reference could be presented 2.2% from Hatton et al [17], 6.1% from Collis and Williams [18], 2.6% from Dennis et al [19] and 2.9% from Badr [20]. To validate the numerical method, comparisons are made with the available

results in the literature for some special cases and the results are found to be in excellent agreement. On the other hand, for the elliptic cylinder, Figure (3) illustrates a comparison of the average Nu for Re in the range of 20 to 200 with Badr [20] under the same conditions: AR=0.6, Pr=0.7, and $\lambda=30^\circ$. The definition of Re is modified to match that of Badr to compare the results easily, and that has been done by relating it to the focal length instead of the major axis length. The comparison shows a good agreement with Badr.

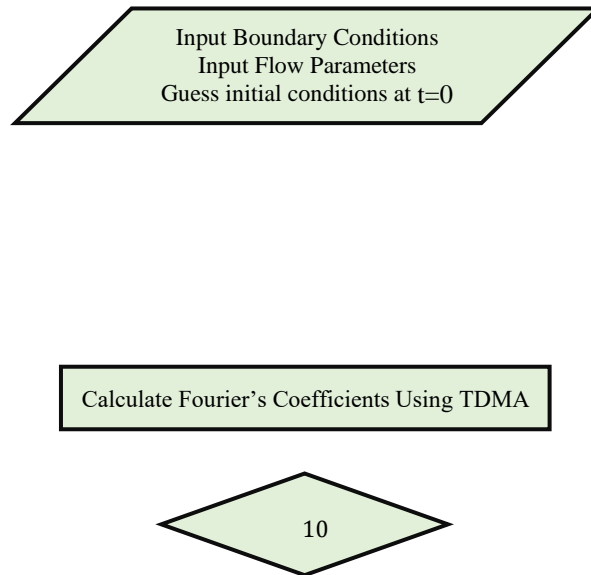


Figure 2- Solution Procedure Flow Chart

Table 2- Comparison of average Nusselt number for forced convection flow over circular cylinder Pr=0.7.

Re	Present AR=0.97	Hatton [17] AR=1	Collis [18] AR=1	Dennis [19] AR=1	Badr [20] AR=0.96
5	1.521	1.561	1.395	1.423	1.456
20	2.632	2.548	2.936	2.557	2.550
40	3.511	3.318	3.185	3.480	3.490

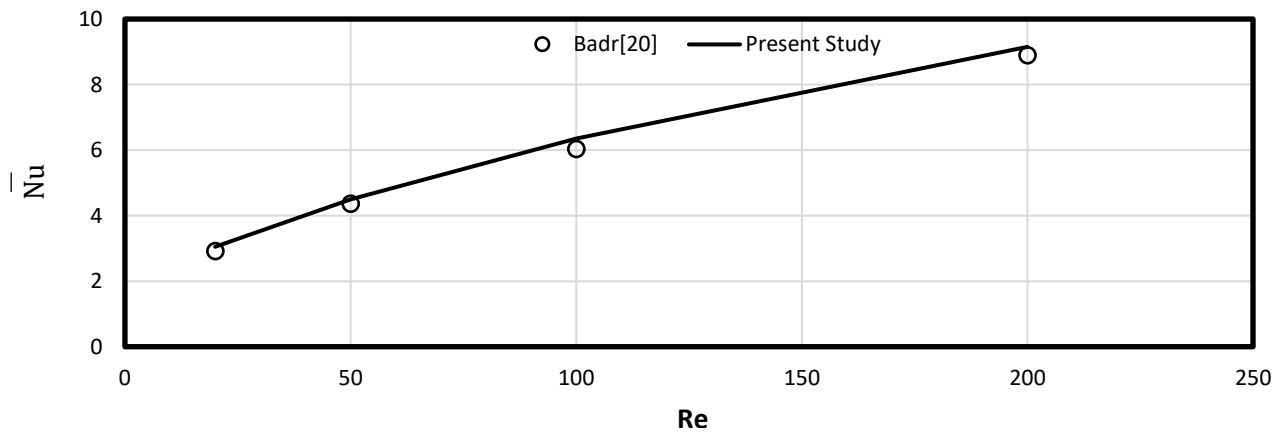


Figure 3- Comparison between the obtained average Nusselt number with Badr [20] for the case AR=0.6, Pr=0.7, and $\lambda=30^\circ$

For the local values of Nu, Figure (4) presents a comparison of the local Nu with Badr [20] for the case AR=0.5, Pr=0.7, $\lambda=0^\circ$, and Re=20, 50, and 100, and the comparison was satisfying.

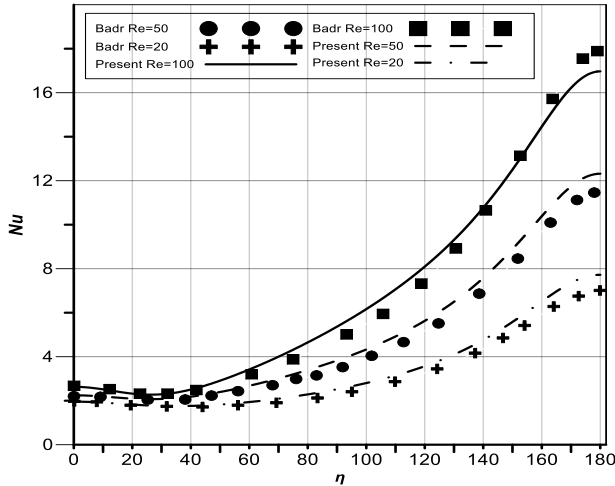


Figure 4- Comparison between the local Nusselt number with Badr [20] for the case AR=0.5, Pr=0.7, $\lambda=0^\circ$, and Re=20, 50, and 100

Figure (5) presents the variation of the local Nusselt number along the elliptical cylinder surface due to nanofluid cross flow at Re=50 with zero angle of inclination and particles volume fraction varies from 0 to 5%. Obviously, the maximum value of Nusselt number is located at the point of stagnation $\eta=180^\circ$ and has a value of 30.35 for water without nanoparticles, 31.61 for nanofluid with 2.5% nanoparticles volume fraction which has an increase of 4.15 % and 32.82 for 5 % volume fraction with an increase of 8.14 %. The comparison shows significant enhancement in Nusselt number along the whole surface. In the direction of flow, the local Nusselt number decreases to find its lowest value at the trailing edge. It can be concluded that, the local Nusselt number increases with increasing ϕ . There is a significant increase in local Nusselt number distribution near the front stagnation region with increasing ϕ . The maximum value of the local Nusselt number occurs at front face of the cylinder facing the incoming flow and decreases gradually over the cylinder surface. This is due to higher thermal gradient and accordingly higher local Nusselt number distribution.

The effect of inclination angle of the tested cylinder on the local Nusselt number is shown in Figure (6). It observed that the Nusselt number exhibits an increase with increasing nanoparticles volume fraction. Maximum value of Nu changes its location slightly with changing λ from 0° to 30° to be at $\eta=185^\circ$, where Nu has a maximum increase of 4.34% for $\phi_p=2.5\%$ and 8.6% for $\phi_p=5\%$. Nusselt number has its lowest

value for all ϕ_p values at $\eta=73^\circ$. Further increase of inclination angle to $\lambda=60^\circ$ shows that, the maximum Nu number changes its position to has its value at $\eta=195^\circ$ and lowest value at $\eta=121^\circ$ but the change of Nu along the surface increases with ϕ_p in some regions and decrease in others as presented in the Figure (7). This may be occurred due the complete period of vortex shedding cycle. Effect of volume fraction of nanoparticles on the local Nusselt number for the case of Re=50, $\lambda=90^\circ$ and AR=0.5 are illustrated in Figure (8). The distribution is almost symmetric and Nu has a maximum value in two locations on the surface at $\eta=210^\circ$ and 340° and the same for the lowest values at $\eta=45^\circ$ and 145° . This may be occurring due the formation of intensified wake vortices behind the vertical cylinder.

Table (3) distinguishes the change in average Nu based on changing angle of inclination and nanoparticles volume fraction. The trend is increasing in average Nu with increasing ϕ_p for all λ values. For instance, there was a maximum increase of 12.4 % under the conditions $\lambda=60^\circ$ and $\phi_p=5\%$. The table discusses the changes of average Nu with changing λ from 0° to 90° , ϕ_p from 0 % to 5 %, Re=50 and AR=0.5. For $\lambda=0^\circ$ the average Nu exhibits the lowest increases with a maximum value of 5.369 % for $\phi_p=5\%$.

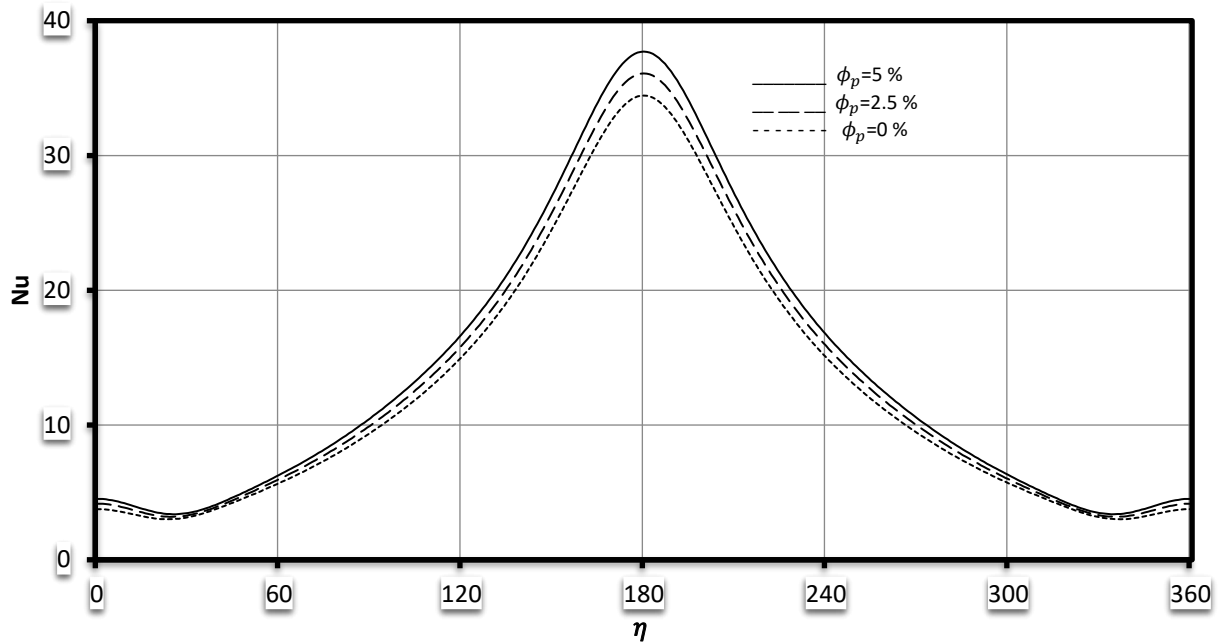


Figure 5- Effect of volume fraction of nanoparticles on the local Nusselt number for the case of $Re=50$, $\lambda=0^\circ$ and $AR=0.5$

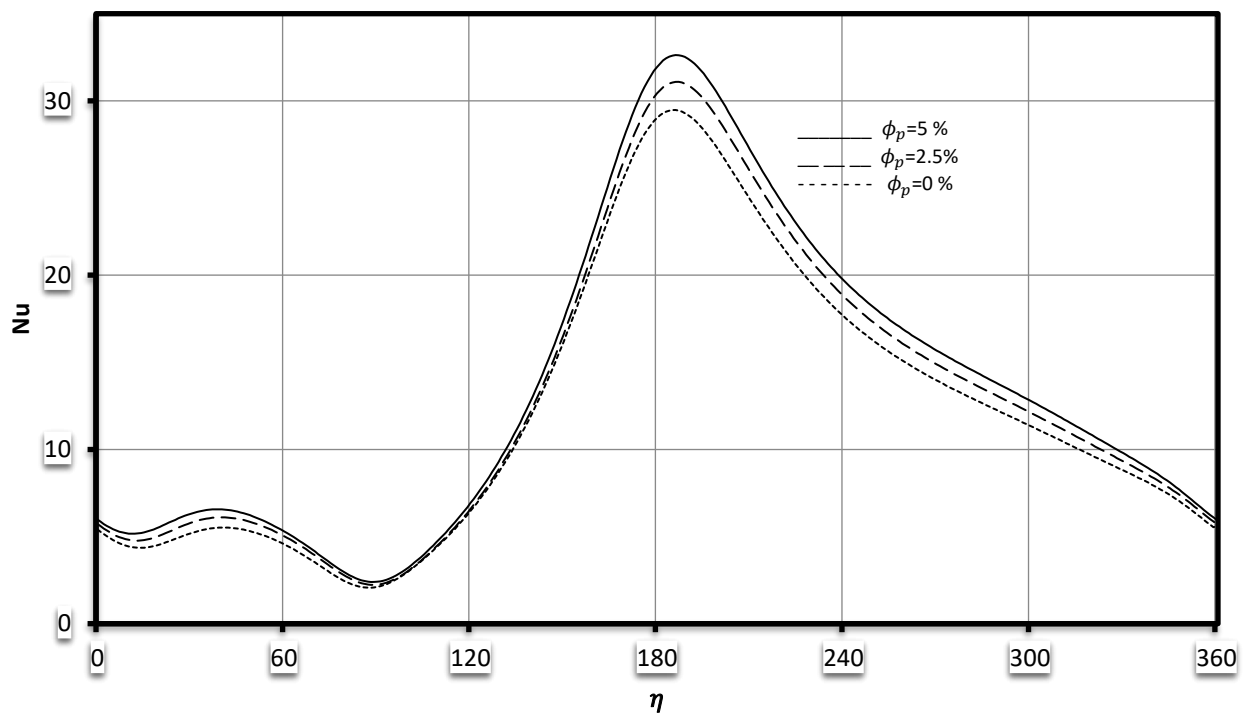


Figure 6- Effect of volume fraction of nanoparticles on the local Nusselt number for the case of $Re=50$, $\lambda=30^\circ$ and $AR=0.5$

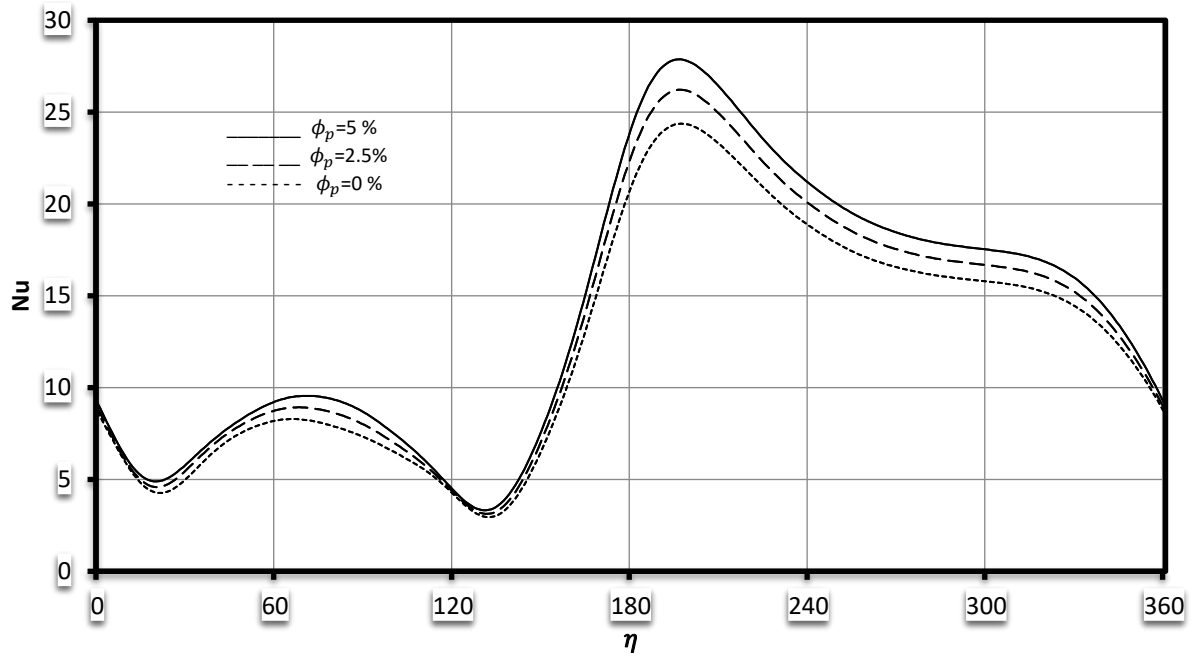


Figure 7- Effect of volume fraction of nanoparticles on the local Nusselt number for the case of $Re=50$, $\lambda=60^\circ$ and $AR=0.5$

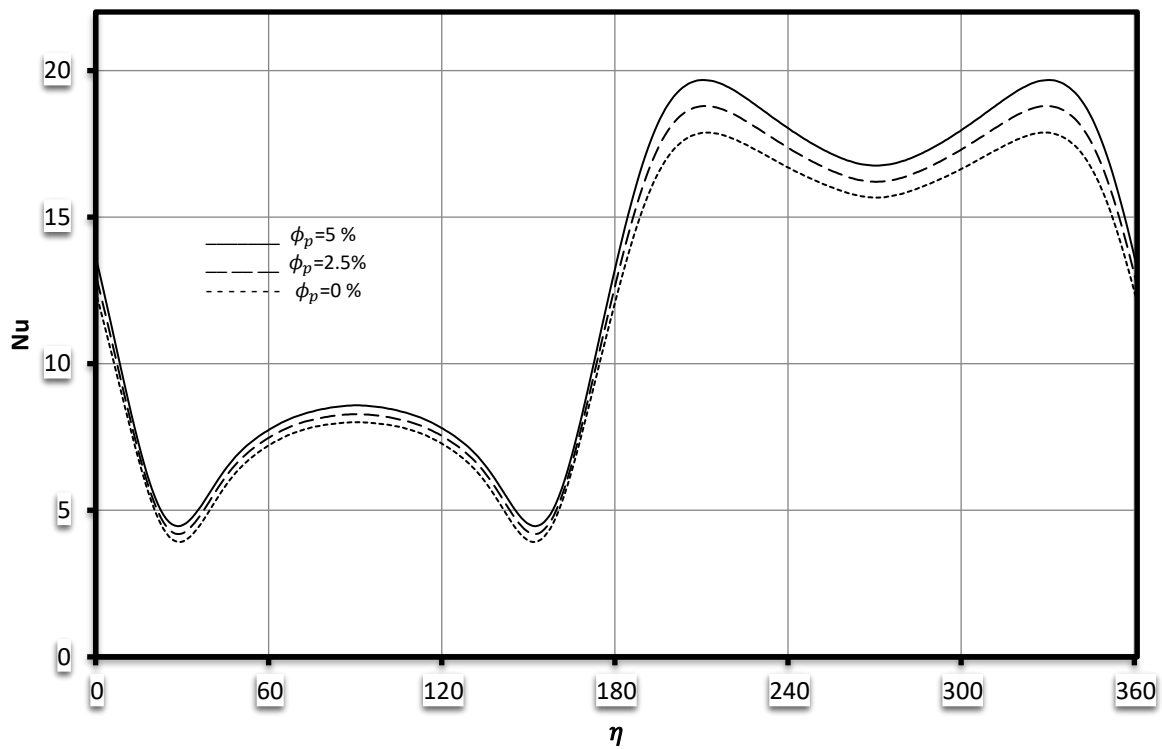


Figure 8- Effect of volume fraction of nanoparticles on the local Nusselt number for the case of $Re=50$, $\lambda=90^\circ$ and AR

Table 3- Effect of angle of inclination and nanoparticles volume fraction of average Nusselt number at Re=50, AR=0.5.

λ	$\% \phi_p$	\bar{Nu}	INCREASE IN NUSSELT
0.0°	0	11.808	0%
	2.5	12.442	5.369%
	5	13.075	10.73%
30°	0	11.127	0%
	2.5	11.780	5.868%
	5	12.397	11.414%
60°	0	11.953	6.417%
	2.5	12.720	0.574%
	5	13.441	12.449%
90°	0	11.421	0%
	2.5	11.906	4.246%
	5	12.395	8.528%

The average Nu with time is introduced in Figure (9) for the case $\lambda=0^\circ$ and in Fig.9 for $\lambda=90^\circ$. The results show the effect of increasing nanoparticles volume fraction on the average Nu, and a significant enhancement is found in Nu value with time in the presented case of Re=50 and AR=0.5.

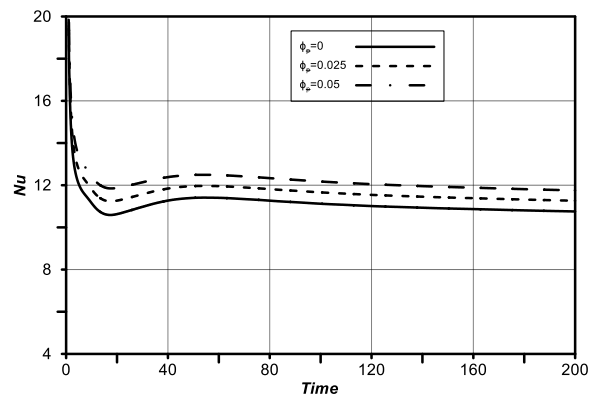


Figure 9- Effect of nanoparticles volume fraction on average Nu in unsteady flow regime for the case Re=50, AR=0.5, and $\lambda=0^\circ$

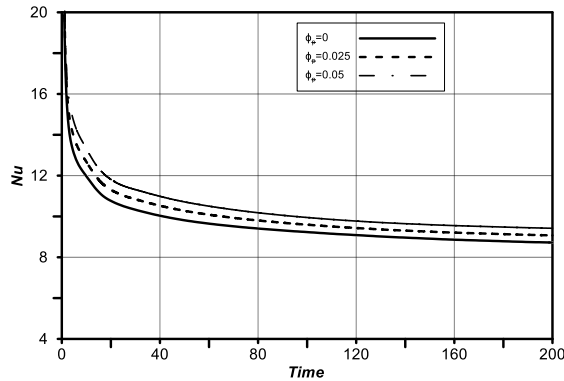


Figure 10- Effect of nanoparticles volume fraction on average Nu in unsteady flow regime for the case $Re=50$, $AR=0.5$, and $\lambda=90^\circ$.

Figure (11) illustrates streamlines pattern for each investigated value of λ . (a) represents $\lambda=0^\circ$ where the streamlines are smooth, and the flow has no wakes in the trailing region as it exhibits a low Re value. The flow regime in (b) where $\lambda=30^\circ$ starts to initiate a wake region but without any vortices. For (c) the angle changed to be $\lambda=60^\circ$ as shown and a single vortex begins to generate in the wake region in the lower half of the regional area. The case $\lambda=90^\circ$ in (d) shows double vortices are generated with symmetric shapes and positions from the center of the cylinder and that happens due to ignoring the gravitational force.

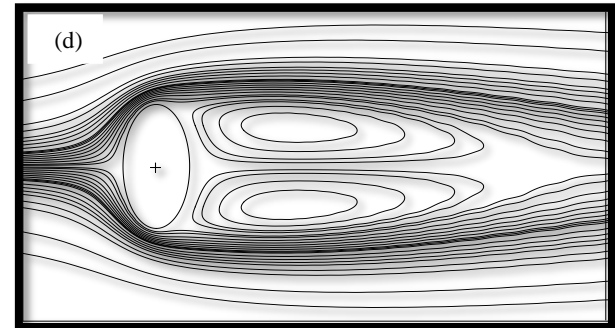
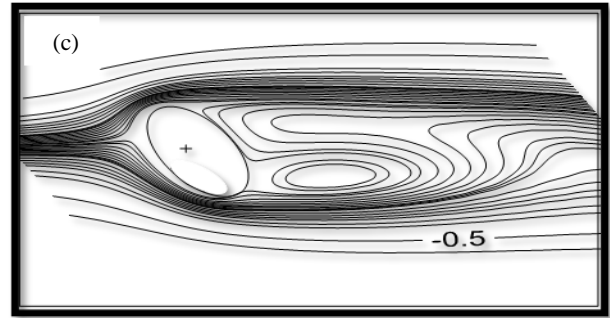
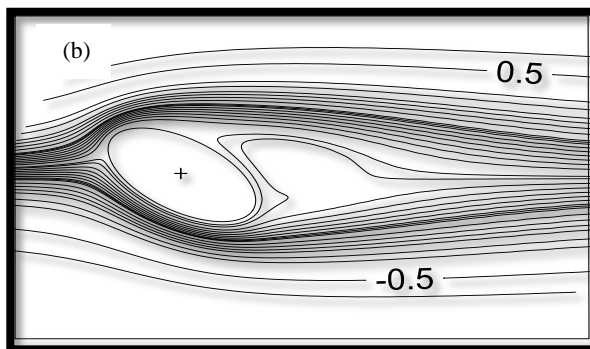
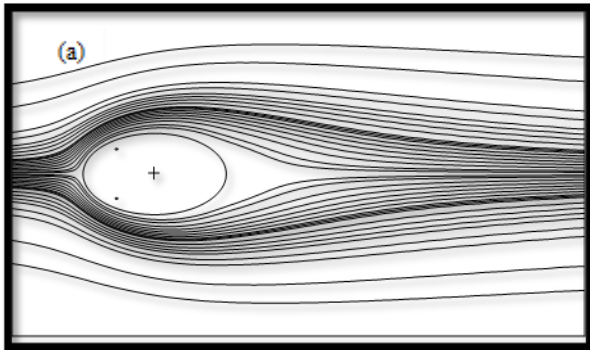


Figure 11- Streamlines patterns for the flow at $Re=50$, (a) $\lambda=0^\circ$, (b) $\lambda=30^\circ$, (c) $\lambda=60^\circ$ and (d) $\lambda=90^\circ$

5. Conclusions

Numerical simulations have been performed to investigate unsteady laminar forced convection from an inclined elliptic cylinder placed in a nanofluid cross laminar flow with constant surface temperature. The nanofluid is created by suspending copper particles in water. The issue of changing the angle of inclination with enhancing the heat transfer rates using nanofluid flow was studied. Inclination angle varies from 0° to 90° , nanoparticles volume fraction occupied the values of 0%, 2.5% and 5% and $Re=50$. The conclusions which can be drawn from this study are:

- 1) The numerical results are validated and comparisons are made with the available results in the published literature for some special cases and the results are found to be in excellent agreement.
- 2) The effect of increasing ϕ_p was as expected to enhance Nu by a significant increase and the maximum increase of 12.4% was detected at $\lambda=60^\circ$ and $\phi_p=5\%$ but for $\lambda=90^\circ$ heat transfer does not enhance in a fulfilling way.
- 3) Increasing the inclination angle tends to enlarge the wake region and the number of vortices increases.
- 4) The time averaged local Nusselt number increases with the concentration of nano-fluid volume fraction (ϕ_p) in unsteady flow regime.

Nomenclature

a	Major Axis
b	Minor Axis
T_s	Cylinder Surface Temperature
λ	Angle of Inclination
U_∞	Far Stream Velocity
T_∞	Far Stream Temperature
u	Velocity Component in x-Direction
v	Velocity Component in y-Direction
Re	Reynolds Number
ϕ	Dimensionless Temperature
ψ	Stream Function
ζ	Vorticity
ν	Kinematic Viscosity
Pe	Peclet Number
C	The Focal Length
ξ	Space Elliptical Coordinate
η	Angular Elliptical Coordinate
μ_{nf}	Nanofluid Dynamic Viscosity
μ_f	Base Fluid Dynamic Viscosity
ϕ_p	Nanoparticles Volume Fraction
ρ_{nf}	Nanofluid Density
ρ_f	Base Fluid Density
k_{nf}	Nanofluid Thermal Conductivity
k_f	Base Fluid Density
α_{nf}	Thermal Diffusivity
h	Convective Heat Transfer Coefficient
Nu	Local Nusselt Number
\overline{Nu}	Average Nusselt Number
L	Ellipse Perimeter

6. References

- [1] Das, S.K., Choi, S.U.S., Yu, W. and Pradeep, T. (2007) *Nanofluids: Science and Technology*, Wiley, Hoboken. <http://dx.doi.org/10.1002/9780470180693>
- [2] Choi S.U.S. and Eastman JA, Enhancing thermal conductivity of fluids, Conference: International mechanical engineering congress and exhibition, San Francisco, CA (United States), 12-17 Nov 1995.
- [3] G. Humnic and A. Humnic, “Application of nanofluids in heat exchangers: A review,” *Renewable and Sustainable Energy Reviews*, vol. 16, no. 8. pp. 5625–5638, Oct. 2012. doi: 10.1016/j.rser.2012.05.023.
- [4] R. Saidur, K. Y. Leong, and H. A. Mohammed, “A review on applications and challenges of nanofluids,” *Renewable and Sustainable Energy Reviews*, vol. 15, no. 3. Elsevier Ltd, pp. 1646–1668, Apr. 01, 2011. doi: 10.1016/j.rser.2010.11.035.
- [5] S. Rashidi, O. Mahian, and E. M. Languri, “Applications of nanofluids in condensing and evaporating systems: A review,” *Journal of Thermal Analysis and Calorimetry*, vol.131, no. 3. Springer Netherlands, pp. 2027–2039, Mar. 01, 2018. doi: 10.1007/s10973-017-6773-7.
- [6] M. N. Khan, W. A. Khan, and I. Tlili, “Forced convection of nanofluid flow across horizontal elliptical cylinder with constant heat flux boundary condition,” *Journal of Nanofluids*, 8 (2019) 386–393, doi: 10.1166/jon.2019.1583.
- [7] S. J. D. D’alessio and S. C. R. Dennis, “Steady laminar forced convection from an elliptic cylinder,” *Journal of Engineering Mathematics*, 29 (1995) 181-193.
- [8] H. M. Badr, “Forced convection from a straight elliptical tube.”, *Heat and Mass Transfer* 34 (1998) 229-236.
- [9] S. A. Patel and R. P. Chhabra, “Forced convection from an inclined elliptical cylinder with constant heat flux: Effect of Prandtl number,” *Lecture Notes in Mechanical Engineering*, pp. 385–394, 2017, doi: 10.1007/978-81-322-2743-4_37.
- [10] C. Sasmal, “Analysis of the effects of inclination angle, nanoparticle volume fraction and its size on forced convection from an inclined elliptic cylinder in aqueous nanofluids,” *Journal of Thermal Analysis and Calorimetry*, vol. 136, no. 3, pp. 1433–1445, May 2019, doi: 10.1007/s10973-018-7750-5.
- [11] W. A. Khan, J. R. Culham, and M. M. Yovanovich, “Fluid Flow Around and Heat Transfer from Elliptical Cylinders: Analytical Approach.”, *Journal of Nanofluids*, 8 (2019) 386–393.
- [12] F. M. Mahfouz, B. M. Maher, and M. K. Yaseen, “Forced Convection from an Isothermal Circular Cylinder Rotating Steadily in a Cross Stream of Nanofluid,” *Mech. Eng.*, vol. 45, no. 2, p. 165, 2022.
- [13] W. M. Collins and S. C. R. Dennis, “Flow past

H. Kotb, F. Mahfouz, M. Abdel-Majeed “Numerical Study of Forced Convection Heat Transfer Across an Elliptic Cylinder in Laminar and Unsteady Nanofluid Flow”

- an impulsively started circular cylinder,” J. Fluid Mech, 60 (1973) 105-127.
- [14] R. K. Tiwari and M. K. Das, “Heat transfer augmentation in a two-sided lid-driven differentially heated square cavity utilizing nanofluids,” International Journal of Heat and Mass Transfer, vol. 50, no. 9–10, pp. 2002–2018, May 2007, doi: 10.1016/j.ijheatmasstransfer.2006.09.034.
- [15] H. C. Brinkman, “The viscosity of concentrated suspensions and solutions,” The Journal of Chemical Physics, vol. 20, no. 4, p. 571, 1952, doi: 10.1063/1.1700493.
- [16] Y. Xuan and Q. Li, “Investigation on convective heat transfer and flow features of nanofluids,” Journal of Heat Transfer, vol. 125, no. 1, pp. 151–155, Feb. 2003, doi: 10.1115/1.1532008.
- [17] A. P. Hatton, D. D. James A N, and D. H. W. Swire, “Combined forced and natural convection with low-speed air flow over horizontal cylinders,” 1970.
- [18] D. C. Collis and M. J. Williams, “Two-dimensional convection from heated wires at low Reynolds numbers.”, Journal of Fluid Mechanics, 6 (1959) 357-384.
- [19] S. C. R. Dennis, J. D. Hudson, and N. Smith, “Steady laminar forced convection from a circular cylinder at low Reynolds numbers,” Physics of Fluids, vol. 11, no. 5, pp. 933–939, 1968, doi: 10.1063/1.1692061.
- [20] H. M. Badr, “Mixed convection from a straight isothermal tube of elliptic cross-section.”, Int. J. Heat Mass Transfer, 37 (1994) 2343-2365
- [21] A.K. Santra, S. Sen, N. Chakraborty, Study of heat transfer augmentation in a differentially heated square cavity using copper–water nanofluid, Int. J. Thermal Sci. 47 (2008) 1113–1122.
- [22] S. Sarkar, S. Ganguly, G. Biswas, Mixed convective heat transfer of nanofluids past a circular cylinder in cross flow in unsteady regime, Int. J. Heat Mass Transfer 55 (2012) 4783–4799.